Vol. 21, No. 1(2022) Cat2602
Revista Mexicana de Ingeniería Química

Experimental measurements of naphta-like hydrocarbons conversion kinetics in an atmospheric dielectric barrier discharge

Medición experimental de la cinética de conversión de hidrocarburos tipo nafta en una descarga de barrera dieléctrica

M.Segura-Ramírez[1]*, M. Nieto-Pérez[2], R. González-Huerta[3], P. Vázquez-Landaverde[2]

[1]*Instituto Politécnico Nacional, CMPL, Av. Acueductos, Ticomán, Gustavo A. Madero, 07340, CDMX, México.*
[2]*Instituto Politécnico Nacional, CICATA Querétaro, Cerro blanco 141, Colinas del Cimatario, 76090, Querétaro, México.*
[3]*Instituto Politécnico Nacional, ESIQIE, Laboratorio de Electroquímica, Unidad Profesional Adolfo López Mateos, CP 07738, CDMX, México.*

Received: September 4, 2021; Accepted: February 3, 2022

Abstract

In the present work, experiments on naptha-like hydrocarbons degradation using arrays of Dielectric Barrier Discharge (DBD) microreactors were performed for the case of high dilution in argon gas and low residence time conditions. A simplified plasma reactor model is presented, and the experimental setup and methodology used to verify the model are presented as well. Experimental conversion data is used to establish a pseudo-first order kinetic constant for the reactor, assuming a plug flow continuous reactor model and using the residence time as the independent variable for the study. Residence time on the experiments was varied by either increasing the length of the reactor (series array) or by splitting the gas flow (parallel array). A rate coefficient of 0.002 s^{-1} was found for the conditions of the experiment. The selectivity and kinetic pathways are beyond the scope of this paper and will be covered in future work; nevertheless, a qualitative assessment of the hydrocarbon degradation products is presented for the experiments carried out.

Keywords: Plasma DBD, Process intensification, Hydrocarbon reforming, Plasma chemistry.

Resumen

En el presente trabajo se realizaron experimentos de degradación en hidrocarburos tipo nafta usando arreglos de microreactores de Descarga de Barrera Dieléctrica para condiciones de una disolución alta en argón y tiempos de residencia bajos. Se presenta un modelo de reactor de plasma simplificado y el arreglo experimental y metodología utilizada para verificar el modelo propuesto. Los datos experimentales de la conversión se utilizan para obtener una constante cinética de pseudo primer orden suponiendo un modelo de flujo tapón continuo para el reactor, dejando para este estudio el tiempo de residencia como una variable independiente. En los experimentos el tiempo de residencia se varió tanto incrementando la longitud del reactor (arreglo en serie) como dividiendo el flujo de gas (arreglos en paralelo). Se encontró una constante cinética de 0.002 s^{-1} para estas condiciones. La selectividad y los posibles caminos cinéticos van más allá del alcance de este trabajo y serán estudiados en futuros trabajos, sin embargo, se muestra una evaluación cualitativa de los productos de degradación en los experimentos que se llevaron a cabo.

Palabras clave: Plasma DBD, procesos de intensificación, reformación de hidrocarburos, química de plasma.

* *Corresponding author. E-mail*: msegurar99@gmail.com
https://doi.org/10.24275/rmiq/Cat2602
ISSN:1665-2738, *issn-e*: 2395-8472

1 Introduction

Today, nearly a quarter of the global energy consumption falls under the transportation sector; and within this sector, 80% of the energy is utilized for freights and passengers transportation. The main form of energy consumption for this activity is in the form of liquid fuels, primarily gasoline and diesel. U.S. Energy Information Administration forecast estimates that global consumption of petroleum and liquid fuels will average 97.7 million barrels per day for all 2021 (U. S. EIA, 2021, Ahmad and Zhang, 2020). It is therefore not surprising that most of the industrial infrastructure for crude oil processing is geared towards the production of liquid fuels.

The landscape, however, is changing: as clean electricity sources become more widespread, the shift from gasoline motorcars to electric vehicles makes more sense every day as a strategy to curb climate change and reduce our energy dependency in fossil fuels for transportation. It is expected that for the year 2030, electric cars will make up 30% of the personal vehicle fleet in all modes, except two-wheelers (IEA, 2020). This change of paradigm will translate into a significant reduction in liquid fuels consumption, which when compounded with a generalized desire to transition towards a sustainable economic activity, will require the rethinking of the oil and gas industry to make it cleaner, more efficient and focused on products other than liquid fuels (Hatfield-Dodds *et al*, 2017).

This reshaping of the oil processing industry opens the door for the implementation of process intensification strategies. Process intensification is a relatively new branch of process engineering, focused mainly in the design of production processes which are substantially smaller, cleaner, safer, and more energy efficient (Stankiewicz and Moulijn, 2000). Energy optimization (Kim *et al*., 2017, Wang *et al*., 2017), green chemistry (Kumar and Nigam, 2012, Sanders *et al*., 2012) process miniaturization and distributed production (Keil, 2018, Tian *et al*., 2018) are examples of process intensification strategies. New technologies that depart from current approaches for chemical process in terms of size (Jaramillo-Gutierrez *et al*., 2021), low cost (Sperandio *et al*., 2022), energy injection (Soto *et al*., 2019) and underlying chemical/biological transformations (Bravo *et al*., 2020) are the trademark of process intensification philosophy. Under this view, the use of electrical discharges to carry out chemical transformations is considered a potential candidate to carry out process intensification (Bogaerts and Neyts, 2018, Gómez-Flores *et al*, 2020).

The chemistry of plasma discharges is radically different to the typical thermal processes in two fundamental aspects: 1) energy injection is mostly electrical and not in the form of heat but rather as an electric field, and 2) the presence of free electrons with average kinetic energies equivalent to temperatures in excess of 10,000 K places these systems far from thermal equilibrium (Meichsner, 2005). Unlike thermal systems, on which most of the chemical processes involve intermolecular collisions, plasma chemistry is dominated by electron-atom and electron-molecule collisions, which leads to processes such as rotovibrational excitation, electronic excitation, bond breaking and ionization (Biberman *et al*., 1982). Also, plasma provide an effective and extremely reactive medium via microfluidic system to generate new species (Lin, 2021). On the downside, plasma chemistry lacks the high selectivity towards a single product typically found in the thermal chemical systems (Adamovich *et al*., 2017).

The effect of plasma on organic molecules has been reported in the literature under two main themes: the use of plasmas as a technology for extracting hydrogen from hydrocarbons (Nishida *et al*., 2014, Wang *et al*., 2016, Biniwale *et al*., 2004, Wang *et al*., 2015) and the abatement of volatile organic compounds (VOC) and other organic pollutants in air or water (Nguyen, 2018, Santos *et al*., 2020, Chang *et al*., 2020, Li *et al*., 2020). It is worth mentioning another emerging branch of plasma catalytic conversion (Ma, 2018), surface modification (Lin, 2021) and removing toxic residues (Balderas-Gutierrez, 2020, Narro-Céspedes, 2020). There are a few reports of applications focused on the processing of streams relevant to oil refining processes (Taghvaei *et al*., 2012, Hueso *et al*., 2009, Khani *et al*., 2014), but compared to the aforementioned applications, the existing studies are scarce. Most of the research cited before is devoted to applying existing DBD technology but not to explore the optimization of reactors structure or the plasma kinetics. The novelty of this work relies in the fact that we use a modular scheme to find a rate coefficient. Also, an evaluation of the plasma efficiency to transform iso-octane into other hydrocarbons and hydrogen is performed. Iso-octane is selected since it is a molecule representative of heavy naphtha streams in refining (Prestvik *et al*., 2004), and the plasma reactor chosen is a dielectric barrier discharge system (Kogelschatz, 2003, Paulmier

and Fulcheri, 2005, Petitpas *et al.*, 2007) since it operates at atmospheric pressure and is therefore more suitable for continuous processes and is cheaper for not requiring vacuum infrastructure.

2 Plasma chemistry processes on gases containing organic molecules

The chemistry of plasma containing hydrocarbons is highly complex, since the molecules are long and their breakage leads to a great variety of fragments. Even with simple hydrocarbons such as propane and propene, the chemistry is highly complex, but still traceable (Dorai, 2002). As the treated hydrocarbons become larger and more complex, establishing specific reaction mechanisms that may yield information on species formed and their abundance becomes a very difficult task. Even the availability of kinetic data for individual species (cross sections and/or rate coefficients) may present a challenge. Therefore, most kinetic modeling efforts of such systems focus on the destruction of reactants and the formation of lumped "pseudoreactants" (Filatov and Kolman, 2006). Most of the work is related to control of VOCs and other organic pollutants, where the main goal of plasma systems is the destruction of the original substance, ensuring at the same time that all by products are inert or easily removed from the treated flow (Vandenbroucke *et al.*, 2011).

A dielectric barrier discharge is created by applying a strong RF electric field to argon gas though a dielectric wall. The discharge typically proceeds in the form of multiple filamentary microdischarges which are a short-lived. The gas ionization produces free charges, and when these charges collide with neutral atoms and molecules in the gas feed new species may be created by electron-induced dissociation. In this way, the pollutant molecules are decomposed into numerous reactive species and radicals. Further degradation occurs by secondary collision between the pollutant molecules and the free radicals and ions formed by previous collisions (Brandenburg *et al.*, 2014). In the end, reaction rate coefficients depend upon plasma parameters, such as Debye length, plasma frequency, degree of ionization and electrical conductivity (Rutscher, 2008).

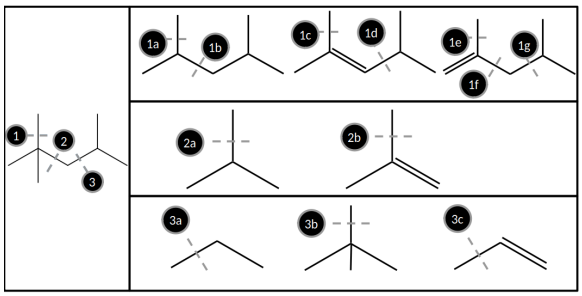

Figure 1. Sequence of iso-octane molecule breaking.

When the gas feed to a DBD plasma reactor contains organic molecules, the high temperature electrons can induce molecule breakage. Typical bond energies present in some hydrocarbon molecules range from 95.6 kcal/mol, 2,2,4 trimethylpentane (iso-octane), to 105.0 kcal/mol, methane. Other hydrocarbons like ethane, propane and butane are in the middle (Luo, 2007). The electron energy in the DBD configurations used in this work was estimated in 3.83×10^{-23} kcal, even if the free electrons in the plasma have a temperature below these values, the high energy tail of the Maxwell-Boltzmann distribution makes molecule breakage possible.

Full kinetic models for the reactions occurring in plasma containing hydrocarbons are highly complex, even for small molecules (Dorai, 2002) and for large species may be untraceable. Figure 1 shows some of the potential breakage mechanisms of the iso-octane molecule, showing that its sequential breakage can lead to fragments between 1 and 16 carbon atoms, since the fragments may recombine with each other to form a very complex hydrocarbon mixture.

3 Simplified plasma reactor model

In order to keep the chemical model simple, only the destruction of the feedstock will be considered, regardless of the products. So a very simplified reaction tree is as follows:

$$A \rightarrow B \tag{1}$$

where A is the original reactant and B is any species other than A. If it is assumed that products B cannot regenerate the reactant species A, the general mass balance equation (1) for the reactor in steady state reduces to a differential equation for the final

concentration in terms of the pseudo first-order rate constant, k, and the volumetric flow, $\dot{V}$. This equation summarized what is usually regarded as standard information of the system under study. Rewriting this differential equation in terms of the residence time, defined as the reactor volume divided by the volumetric flow rate and solving led us to

$$\frac{dX_A}{d\tau} = k(1 - X_A) \tag{2}$$

Equation (2) is separable and readily solved to yield the following expression for the conversion as a function of residence time:

$$X_A = 1 - e^{-Da} \tag{3}$$

where Da is the Damkohler number. The Damkohler number can be found if the conversion is known for a particular reactor configuration:

$$Da = -\ln(1 - X_A) \tag{4}$$

And by definition, for a first order reaction such as the one considered here the Damkohler number is also given by:

$$Da = k\tau \tag{5}$$

It is clear from equations (4) and (5) that a plot of the Damkohler number, obtained from eq. (4), versus residence time will yield a straight line with slope k, which is the parameter that we aim to find in this study.

4 Experimental setup

4.1 DBD unit reactor

The base DBD reactor is constructed with a coaxial configuration, using a quartz tube with 3.7 mm ID, 1.2 mm wall thickness and 150 mm length. The small radius was chosen since a smaller electrode separation favors a higher electron temperature in the plasma. The inner (powered) electrode is a 304 stainless steel rod with 1.3 mm in diameter and 130 mm long, welded to a 0.25 inch steel stub used for electrode mounting. The outer (grounded) electrode is aluminum tape wrapped around the outer surface of the quartz tube. This results in a plasma volume of 1.6 cm^3 for this single reactor. Commercial push-to-connect pneumatic fittings for 0.25-inch tubing are used to connect the reactor body, the electrode and to feed gas. These type of modular construction of a single reactor allows for easy arrangement of multiple reactors with respect to flow in series, in parallel or in series/parallel combinations.

4.2 Electrical power supply

Power is supplied to the reactor through a high voltage, high frequency power supply, which consists of a rectifying unit, a variable high-frequency inverter using two mosfet transistors in a half-bridge configuration, and a high-frequency transformer for voltage elevation 20:1. This power supply can provide sinusoidal high voltage waveforms with frequencies in the range 10-100 kHz and peak-to-peak voltages up to 20 kV. In all the experiments in this work, peak-to-peak voltage amplitude was set to 5 kV and the frequency was set to 25 kHz, which was the resonant condition that enabled the most transfer of power to the reactor electric load. The voltage level was set to 5 kV to keep the electrical discharge confined to the interior of the tube and avoid arcing between the inner electrode and the metallic gripping mechanism of the fittings used to construct the reactor. More details on the power supply construction and operation can be found elsewhere (Soto-Ruvalcaba, 2014).

4.3 Conversion measurement experimental setup

The experimental setup and a schematic showing the main components of reactor can be seen in Figure 2. Due to its low dielectric strength, argon gas is used as working gas. Thus, as iso-octane is highly diluted in argon, the breakdown voltage is expected to reduce. Carrier gas is argon provided by Infra, grade Sparklaser Protect-M (99.995 % purity), shown as TA-101 in the diagram. The gas coming from the cylinder is split into two currents, regulated by valves V-101 and V-102. After each valve, an electronic flow meter is placed to monitor the flow during experiments: the F-101 meter (MKS M10MB, 0-200 sccm) is placed after V-101, and the F-102 meter (Omega FMA3107, 0 -2000 sccm) is connected to V-102. The analog signal from both F-101 and F-102 flowmeters is monitored and recorded on a PC using an Arduino Mega 2560 data acquisition card.

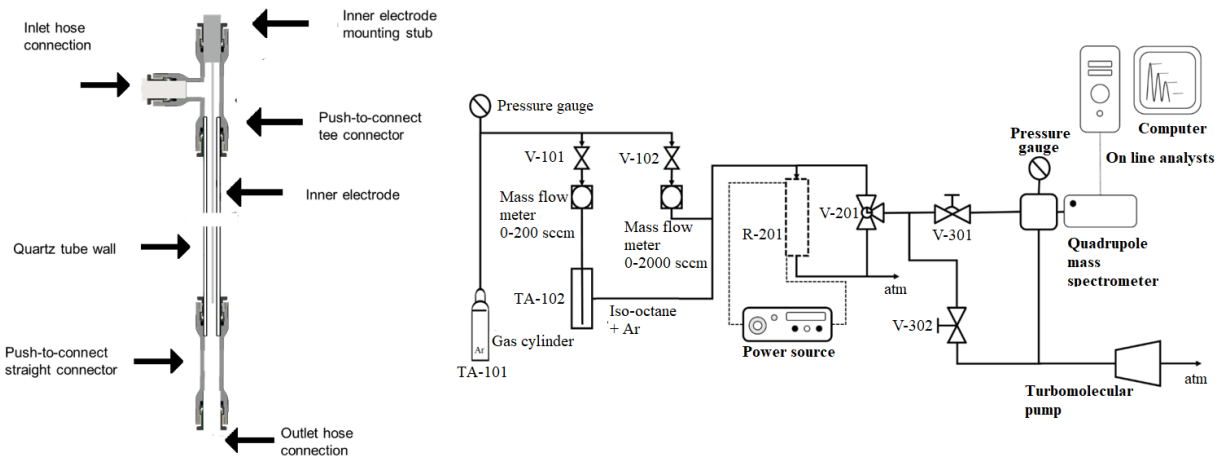

Figure 2. Schematic of the DBD coaxial reactor showing its main components and experimental setup to evaluate the conversion efficiency of a DBD plasma.

For these experiments it is assumed that the argon gas is completely saturated with iso-octane vapor as it passes through the gas bubbler TA-102. The solvent-saturated gas output of TA-102 is mixed with the pure argon stream coming from V-102, and the mixture is fed into the DBD reactor bank R-201, and the output is sent to a fume hood with air extractor. A four-way toggle valve V-201 (Swagelok SS-43Z6FS1) allows connection to the sampling line to either the input of R-201, the output of R-201 or to a blind connection. The valve V-301 is a fine leak valve (Kurt J. Lesker VZLVM940R) which allows fine regulation of a gas ingress into a small vacuum chamber equipped with a miniature quadrupole mass spectrometer (QMS, HORIBA STEC Micropole system, sensor SMPA7-7-2/65 K, spectrum generator QL-SG01-065-1A) which can identify residual gas species in the range 2 - 65 amu. The valve V-302 is used to connect the sampling line directly to the vacuum pump in order to purge it when V-201 is open to its blind port and V-301 is closed.

In a typical experiment, either the input or the output of R-201 is monitored for 5 to 10 minutes by setting V-201 to the corresponding position. V-301 is opened to give an adequate signal of the masses of interest, taking care of keeping the total pressure below 10^{-5} torr in the vacuum chamber to protect the QMS. Once the monitoring is complete, V-201 is moved to its blind position, V-301 is closed and V-302 is opened; this purges the sampling line, leaving it ready for another measurement. After 3 to 5 minutes of purge, V-302 is closed and V-201 can now be moved to either the input or the output of R-201. V-301 is opened to the same setting and the new monitoring round starts. Isoctane concentration on gas stream was determined measuring the mass of isoctane before and after argon enters the bubbler for three different times. Once the mass difference is known the molar number is determined via Antoine coefficients (Yaws, 2015).

4.4 Solvent conversion analysis

During sampling, the QMS shows signal intensities associated with the values of m/q for the species produced in the ionizer, which can be used to estimate partial pressures of the species present in the sampling line. The main mass signals in the reactor inlet flow are 40, which corresponds to the Ar carrier gas, 28 associated with air impurities in the system, 18 for water vapor, and masses 43, 56 and 57, which correspond to the main mass peaks of isooctane spectra (NIST, 2021). Table 1 presents the relative intensities of the masses relevant to the isooctane, both from the literature (NIST, 2021) and from experiments of pure iso-octane vapor injection to the measuring system.

During actual experiments, masses in the range 38-42 on Table 1 are inaccessible during the experiments due to the presence of the large Ar peak at mass 40, which the mass spectrometer cannot resolve adequately.

Once the relevant masses are identified, they are tracked as a function of time by the QMS. Each sampling lasts between 10 and 15 minutes, which allows collecting up to 12 data points for each mass.

Table 1. Comparison between relative intensity of main masses.

m/z	Mass peaks relative intensities	
	Reported (NIST, 2021)	Measured
38	30	484.04
39	559	1257.45
40	109	1085.75
41	2129	3343.94
42	129	2124.37
43	1849	2262.4
56	3339	6394.98
57	9999	9999

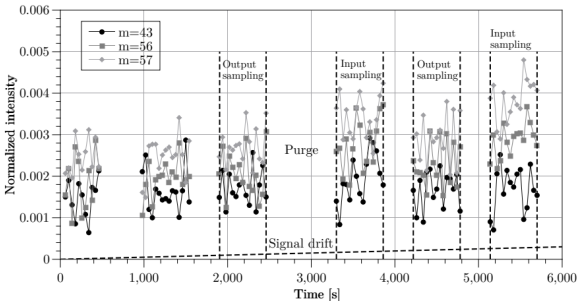

Figure 3. Time evolution of the mass associated to isooctane during an experiment. Multiple samples of reactor input and output are taken during the experiment, and a slow linear drift upwards is clearly seen and subtracted during the analysis. The empty spaces between samplings correspond to sampling line purging periods.

Mass intensities are normalized to mass 40, corresponding to the Ar gas carrier, and then the average and standard deviation value for each mass during the sampling period are recorded, removing any baseline drift. During the experiment, samplings of both reactor input and output are recorded. Time evolution of the relevant masses during a typical experiment is shown in Figure 3. The sampling periods of input and output are clearly visible, separated by the purge of the sampling line where all masses drop to really low values. Intensities for equation (6) are obtained by averaging data over the sampling period, and the standard deviation is used as the error during the sampling period.

Since the normalized signal for the main isooctane mass I_{57} is measured at both entrance and exit, the isooctane conversion is calculated as:

$$X_{A,f} = 1 - \frac{I_{57,in}}{I_{57,out}} \tag{6}$$

Residence time for the experiment is calculated by dividing the reactor volume over the flow rate. For a configuration with reactors in series, the volume is the product of an individual reactor times the number of reactors, and the flow used to calculate the residence time is simply the total gas flow. For parallel reactor arrays, the volume used to calculate the residence time is the volume of the individual reactor, and the flow is equal to the total flow divided by the number of parallel branches. Once conversion and residence time have been calculated, a plot of X_A vs τ can be generated to see if it adjusts to equation (6).

5 Results

5.1 *Determination of the first order rate constant*

Experiments were carried out in both series and parallel configurations, to detect any deviation from the simple first order mechanism. For the reactors in series experiments, the gas flow was kept at values around 19 cm^3/s, which represent an initial iso-octane concentration of $5\times10^{-5} \pm 0.25\times10^{-5}$ mol/s according to the calculations from Section 4.3. A single reactor represents a volume of 1.6 cm^3, so two reactors in series have a volume of 3.2 cm^3. The error in the flow rate was determined from the fluctuations of the electronic mass flow meters during the sampling, and the volume error was assumed to be 5% for each reactor. Complementary experiment with three reactors in parallel array represent a total reaction volume of 4.8 cm^3 and were fed with varying flow rates between 5 and 15 cm^3/s; it was assumed that the total flow and the solvent input is divided between the three reactors equally.

The residence time range explored during this study was therefore between 100 and 300 ms. Table 2 presents the conditions for the 10 experiments performed, as well as the value of conversion obtained in each case.

Conversion was calculated using equation (6), and the error is obtained from the standard deviation of the corresponding mass intensity during the sampling period.

According to equation (3), if the degradation of iso-octane follows a first order kinetics with a constant rate coefficient, a plot of $\ln(1 - X_A)$ vs residence time should be a straight line, and the slope of that line would yield the first order rate coefficient; moreover, if equation (3) holds, data from series and parallel

Table 2. Summary of the experiments carried out during this study, showing the values of the independent variable (residence time) and the dependent variable (conversion).

Configuration	Volume (cm^3)	Flow rate (cm^3/s)	Residence time, t (ms)	Conversion, XA (\%)
Series	1.6 ± 0.08	19.96 ± 0.17	81± 4	21 ± 0.01
Series	3.2 ± 0.16	19.70 ± 0.21	164 ± 9	30 ± 0.01
Series	3.2 ± 0.16	18.41 ± 0.18	175 ± 10	31 ± 0.04
Series	4.8 ± 0.24	18.30 ± 0.31	264 ± 13	38 ± 0.05
Series	4.8 ± 0.24	18.35 ± 0.30	264 ± 13	39 ± 0.06
Parallel	1.6 ± 0.08	5.83 ± 0.23	276 ± 20	37 ± 0.05
Parallel	1.6 ± 0.08	6.31 ± 0.21	255 ± 17	41 ± 0.03
Parallel	1.6 ± 0.08	6.88 ± 0.20	234 ± 13	23 ± 0.01
Parallel	1.6 ± 0.08	13.70 ± 0.30	118 ± 6	25 ± 0.06
Parallel	1.6 ± 0.08	7.18 ± 0.20	225 ± 15	52 ± 0.15

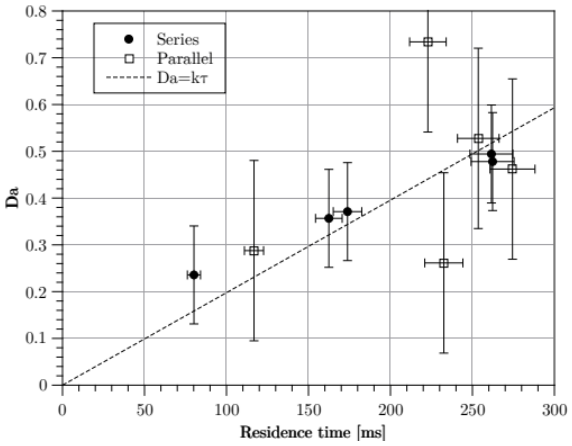

Figure 4. Calculation of the first order rate constant for the degradation of isooctane in the DBD microreactor. According to eq. (3), the slope of the fitted line passing through the origin in this plot represents the rate constant. No appreciable difference in the value was found between the series and parallel configurations, suggesting that the rate coefficient is constant along the reactor.

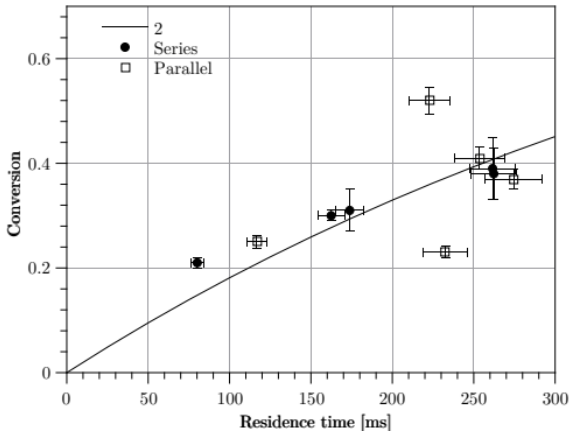

Figure 5. Comparison between the experimental data and the first order constant rate coefficient model for a value of k = 0.002, obtained from the linear fits in Figure 4.

reactor arrays should adjust to the same straight line. Figure 4 presents such plot, showing the cases of series and parallel reactors arrays separately.

Linear fits were performed on the two data sets and are shown in the Figure 4 as well; for the reactors in series case, the data adjusts to a straight line, with a slope of 0.002 s^{-1}. The data for parallel reactors shows more dispersion, but the straight line fit to this data also yields a value of 0.002 s^{-1}. This plot shows that in this range of residence time, the kinetics of iso-octane degradation can be described with a first order reaction with a rate coefficient of 0.002 s^{-1}. Since the plasma properties are a function of the gas composition, it is expected that experiments with higher concentration of solvent will not show this behavior, since in that case the rate coefficient will certainly vary as conversion progresses.

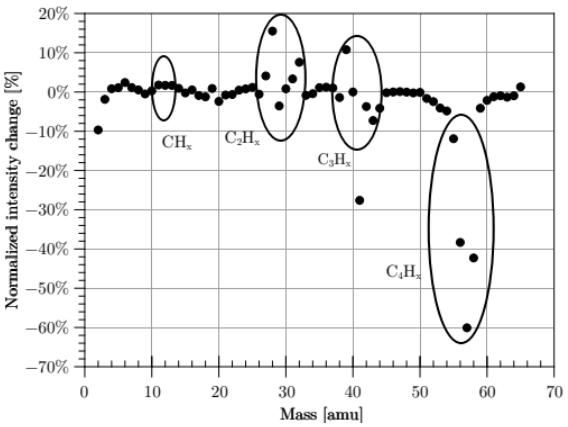

Figure 6. Percent change of masses in the system, normalized to the main solvent input intensity. Mass ranges where fragments with the given number of carbons are encircled.

In this case, the level of dilution in this experiment is so low that this effect is negligible.

With the value of the rate constant known, the conversion curve can be generated for this high solvent dilution case studied here. Figure 5 shows a comparison of the experimental conversion data with the prediction of the first order model using the value of k obtained from Figure 4.

Again, it can be seen that the experimental points corresponding to parallel reactors show a greater scatter; this may be caused by uneven gas or solvent flow partition. The data for reactors in series shows very good agreement with the first order kinetics model.

5.2 Qualitative assessment of iso-octane degradation products

With the quadrupole available to measure conversion, it is difficult to make a quantification of the solvent fragments with less than 4 carbon atoms. However, some evidence of solvent fragmentation can be observed. Figure 6 shows the percent change in masses between input and output for an experiment where 40% solvent conversion was achieved.

The reduction of the main solvent peak is consistent with 40% conversion, and an increase of intensities in the mass range 28 - 32 is observed between the input and the output, consistent with formation of C2 fragments. Methane and methyl fragments are not observed, and in the case of C3 the carrier gas signal interferes to make a viable qualitative statement.

In addition to the in-line measurements using the QMS, off-line composition analysis of aliquots from reactor input and output were performed in a gas chromatograph (GC). Aliquots were analyzed by gas chromatography coupled to mass spectrometry detection on an Agilent 7890A GC System (Agilent Technologies, Inc., Santa Clara, CA) equipped with an Agilent 5975C VL mass selective detector. Headspace extraction was performed with multi-purpose autosampler MPS2 XL (Gerstel Inc., Linthicum, MD), incubating vials at 80 °C for 2 min, and suction of 2 ml with a gas-tight syringe. The separation of the samples was carried out on a DB-1 capillary column (25 m long, 0.32 mm diameter, and 0.52 micron phase wide, Agilent Technologies) using helium as carrier gas at a flow rate of 1 ml/min (purity 99.999%). The GC injector was held at 250 ºC with split ratio 1:1 and the Mass Spectrometer set on Electron Impact mode at 70 eV, Gain Factor 1, transfer line temperature at 280 °C, ion source at 230 °C and quadrupole at 150 °C. Mass range 8-200 uma. The oven temperature started at 40ºC and held for 10 min, then 40 ºC/min from 40 to 260 ºC. Data analysis was done with MSD ChemStation software v. E.02.00.493 (Agilent Technologies). Compounds identification performed by comparing spectral data with those of the NIST/EPA/NIH Mass Spectra Library, version 1.7, USA. Four aliquots for GC analysis were taken in vials, one for the input current and three for the output current. These analyses allowed for a more detailed identification of byproducts and an additional estimate of the rector conversion value. Quantitatively, this estimate agrees with the percent change showing a relative abundance of 46.23% in iso-octane and the appearance of 57.77% light hydrocarbons, molecules with 2, 3 and 4 carbon atoms. These lighter hydrocarbons are hard to identify in QMS due to their similarities with another molecules. Along with this abundance group some compounds were identified in minimum percentage, which ranging from molecules with seven to sixteen carbon atoms.

Conclusions

Experiments on iso-octane degradation using arrays of dielectric barrier discharge microreactors were performed for the case of high dilution in argon gas and low residence time conditions. It was found that for these conditions the degradation follows a first order kinetic mechanism, with a rate coefficient

of 0.002 s^{-1}. Since no significative differences were found between series and parallel arrays of reactors, it can be inferred that no axial variation occurs and the electron density could be assumed as constant, as well as the rate constant. Parallel arrays of reactors show a slight scatter for these particular operating conditions; however, same conclusions can be made. It is expected that at higher solvent concentrations this will not be the case due to the influence of the solvent on plasma properties; this hypothesis will be the subject of a subsequent work.

From gas chromatoghrapy we can see different species presents in gas stream, most of them corresponding to C7-C16 hydrocarbons. This is a result from the degradation of isooctane into smaller pieces. Nevertheless, these pieces can recombine to form heavier species, giving as result molecules in the C10-C16 range. This can be interpreted as process of isomerization were bigger molecules can be created through smaller ones. Lighter hydrocarbons are hard to distinguish due to the characteristics of the column used for GC-MS. Precise test must be run to identify a specific lighter hydrocarbon.

Acknowledgments

The authors would like to thank the IPN multidisciplinary project SIP-2181 (2022-2024) and Ciencia Basica Project A1-S-15770. Miguel Ángel Segura acknowledges CONACYT for the scholarship.

References

Adamovich, I., Baalrud, S. D., Bogaerts, A., Bruggeman, P. J., Cappelli, M., Colombo, V., Czarnetzki, U., *et. al*, (2017). The 2017 Plasma Roadmap: Low temperature plasma science and technology. *Journal of Physics D: Applied Physics 50(32)*, 323001. https://doi.org/10.1088/1361-6463/aa76f5

Ahmad, T., Zhang, D. (2020). A critical review of comparative global historical energy consumption and future demand: The story told so far. *Energy Reports 6*, 1973-1991. https://doi.org/10.1016/j.egyr.2020.07.020

Aitani, A. M. (2007). *Catalytic Naphtha Reforming*. Second Edition, Revised and Expanded (English Edition) (2nd Revised edition). Dekker.

Balderas-Gutiérrez, J., Hernández-Tenorio, C., Zavala-Arce, R., Pacheco-Sánchez, J., García-Gaitán, B., Illescas, J. (2020). Chitosan films modified with glow discharge plasma in aqueous solution of pyrrole and its evaluation in the removal of red dye no. 2. *Revista Mexicana de Ingeniería Química 19(3)*, 1291-1299. https://doi.org/10.24275/rmiq/ia893

Biberman, L. M., Vorob'Ev, V. S., Yakubov, I. T. (2012). Kinetics of Nonequilibrium Low-Temperature Plasmas (Reprint ed.). Springer.

Biniwale, R. B., Mizuno, A., Ichikawa, M. (2004). Hydrogen production by reforming of iso-octane using spray-pulsed injection and effect of non-thermal plasma. *Applied Catalysis A: General 276(1-2)*, 169-177. https://doi.org/10.1016/j.apcata.2004.08.003

Bogaerts, A., Neyts, E. C. (2018). Plasma technology: An emerging technology for energy storage. *ACS Energy Letters 3(4)*, 1013-1027. https://doi.org/10.1021/acsenergylett.8b00184

Brandenburg, R., Kovačević, V. V., Schmidt, M., Basner, R., Kettlitz, M., Sretenović, G., Obradović, B., Kuraica, M., Weltmann, K. D. (2014). Plasma-based pollutant degradation in gas streams: Status, examples and outlook. *Contributions to Plasma Physics 54(2)*, 202-214. https://doi.org/10.1002/ctpp.201310059

Bravo, S., Torres-González, J., Morales-Hernández, J., Martínez-Franco, E., González-Olvera, J., Mercader-Trejo, F., Rodríguez-López, A., Manzano-Ramírez, A., Esparza, A., Herrera-Basurto, R. (2020). Effect of the manufacturing parameters on the quality of the ceramic thermal barrier coating after ageing by thermal treatment. *Revista Mexicana de Ingeniería Química 20(1)*, 227-237. https://doi.org/10.24275/rmiq/Mat1041

Chang, Z., Wang, C., Zhang, G. (2020). Progress in degradation of volatile organic compounds based on low-temperature plasma technology. *Plasma Processes and Polymers 17(4)*, 1900131. https://doi.org/10.1002/ppap.201900131

Dorai, R. (2002). *Modeling of atmospheric pressure plasma processing of gases and*

surfaces. Ph. D. Thesis in Chemical and Biomolecular Engineering, University of Illinois at Urbana-Champaign, USA. https://uigelz.eecs.umich.edu/pub/theses/rajesh_phd_thesis.pdf

Filatov, I. E., Kolman, E. V. (2006). Formal kinetic description of VOCs removal by plasma methods. *Journal of Physics: Conference Series 44*, 155-161. https://doi.org/10.1088/1742-6596/44/1/021

Gómez-Flores, P., Velasco-Álvarez, N., González, I., Sánchez-Vázquez, V. (2020). Biotechnological processes improved with electric fields: the importance of operational parameters selection. *Revista Mexicana de Ingeniería Química 19*(Sup. 1), 111-121. https://doi.org/10.24275/rmiq/Bio1689

Hao, W., Ling-Jun, S., Xing-Hu, L., Li-Meng, Y. (2015). Hydrogen production from partial oxidation of methane by dielectric barrier discharge plasma reforming. *Acta Physico-Chimica Sinica 31(7)*, 1406-1412. https://doi.org/10.3866/pku.whxb201504272

Hatfield-Dodds, S., Schandl, H., Newth, D., Obersteiner, M., Cai, Y., Baynes, T., West, J., Havlik, P. (2017). Assessing global resource use and greenhouse emissions to 2050, with ambitious resource efficiency and climate mitigation policies. *Journal of Cleaner Production 144*, 403-414. https://doi.org/10.1016/j.jclepro.2016.12.170

Hippler, R., Kersten, H., Schmidt, M., Schoenbach, K. H. (2008). *Low Temperature Plasmas: Fundamentals, Technologies and Techniques*. (2nd Revised ed.). Wiley-Vch.

Hueso, J. L., Rico, V. J., Cotrino, J., Jiménez-Mateos, J. M., González-Elipe, A. R. (2009). Water plasmas for the revalorisation of heavy oils and cokes from petroleum refining. *Environmental Science & Technology 43(7)*, 2557-2562. https://doi.org/10.1021/es900236b

IEA. (2020). *Global EV Outlook 2020 - Analysis*. https://www.iea.org/reports/global-ev-outlook-2020

Jaramillo-Gutiérrez, M., Pedraza-Avella, J., González, I., Rivero, E., Cruz-Díaz, M. (2021). Design equations based on micro/macromixing theoretical analysis of RTD curves for a tubular concentric electrochemical reactor with expanded meshes as electrodes. *Revista Mexicana de Ingeniería Química 21(1)*, Cat2434. https://doi.org/10.24275/rmiq/Cat24334

Keil, F. J. (2017). Process intensification. *Reviews in Chemical Engineering 34(2)*, 135-200. https://doi.org/10.1515/revce-2017-0085

Khani, M. R., Khosravi, A., Dezhbangooy, E., Hosseini, B. M., Shokri, B. (2014). Study on the feasibility of plasma (DBD reactor) cracking of different hydrocarbons (-hexadecane, lubricating oil, and heavy oil). *IEEE Transactions on Plasma Science 42(9)*, 2213-2220. https://doi.org/10.1109/tps.2014.2345846

Kim, Y. H., Park, L. K., Yiacoumi, S., Tsouris, C. (2017). Modular chemical process intensification: A review. *Annual Review of Chemical and Biomolecular Engineering 8(1)*, 359-380. https://doi.org/10.1146/annurev-chembioeng-060816-101354

Kogelschatz, U. (2003). Dielectric-barrier discharges: Their history, discharge physics, and industrial applications. *Plasma Chemistry and Plasma Processing 23(1)*, 1-46. https://doi.org/10.1023/a:1022470901385

Kumar, V., Nigam, K. D. P. (2012). Process intensification in green synthesis. *Green Processing and Synthesis 1(1)*. https://doi.org/10.1515/greenps-2011-0003

Li, S., Dang, X., Yu, X., Abbas, G., Zhang, Q., Cao, L. (2020). The application of dielectric barrier discharge non-thermal plasma in VOCs abatement: A review. *Chemical Engineering Journal 388*, 124275. https://doi.org/10.1016/j.cej.2020.124275

Lin, L., Quoc Pho, H., Zong, L., Li, S., Pourali, N., Rebrov, E., Nghiep Tran, N., Ostrikov, K. K., Hessel, V. (2021). Microfluidic plasmas: Novel technique for chemistry and chemical engineering. *Chemical Engineering Journal 417*, 129355. https://doi.org/10.1016/j.cej.2021.129355

Lin, L., Rui, L., Li, C., Liu, Q., Li, S., Xia, Y., Hu, H., Yang, W., Xu, H. (2021).

Study on CO_2-based plasmas for surface modification of polytetrafluoroethylene and the wettability effects. *Journal of CO_2 Utilization 53*, 101752. https://doi.org/10.1016/j.jcou.2021.101752

Luo, Y. R. (2007). *Comprehensive Handbook of Chemical Bond Energies*. Amsterdam University Press.

Ma, X., Li, S., Ronda-Lloret, M., Chaudhary, R., Lin, L., van Rooij, G., Gallucci, F., Rothenberg, G., Raveendran Shiju, N., Hessel, V. (2018). Plasma assisted catalytic conversion of CO_2 and H_2O over Ni/Al_2O_3 in a DBD reactor. *Plasma Chemistry and Plasma Processing 39(1)*, 109-124. https://doi.org/10.1007/s11090-018-9931-1

Meichsner, J. (2005). Low temperature plasmas. In *Plasma Physics* (pp. 95-116). Springer, Berlin, Heidelberg. https://doi.org/10.1007/11360360_5

Meichsner, J., Schmidt, M., Schneider, R., Wagner, H. (2012). *Nonthermal Plasma Chemistry and Physics*. (English Edition) (1st. ed.). CRC Press.

Narro-Céspedes, R., Reyna-Martinez, R., Ibarra-Alonso, M., Narro-Céspedes, R., Martínez-Luevanos, A., Zugasti-Cruz, A., Neira-Velazquez, M., Sánchez-Valdés, S., Soría-Arguello, G., Reyes-Acosta, Y. (2020). Effect of thermal and argon plasma treatment in SiO_2 spheres, assessing the effectiveness in the elimination of organic waste. *Revista Mexicana de Ingeniería Química 19(3)*, 1071-1081. https://doi.org/10.24275/rmiq/mat906

Nguyen, H. P., Park, M. J., Kim, S. B., Kim, H. J., Baik, L. J., Jo, Y. M. (2018). Effective dielectric barrier discharge reactor operation for decomposition of volatile organic compounds. *Journal of Cleaner Production 198*, 1232-1238. https://doi.org/10.1016/j.jclepro.2018.07.110

Nishida, Y., Chiang, H. C., Chen, T. C., Cheng, C. Z. (2014). Efficient production of hydrogen by DBD type plasma discharges. *IEEE Transactions on Plasma Science 42(12)*, 3765-3771. https://doi.org/10.1109/tps.2014.2354695

NIST Mass spectrometry data center. (2021). Mass Spectra. In W. E. Wallace (Ed.), *NIST Chemistry WebBook* (Vol. 69, pp. 1-2). NIST.

Paulmier, T., Fulcheri, L. (2005). Use of non-thermal plasma for hydrocarbon reforming. *Chemical Engineering Journal 106(1)*, 59-71. https://doi.org/10.1016/j.cej.2004.09.005

Petitpas, G., Rollier, J., Darmon, A., Gonzalez-Aguilar, J., Metkemeijer, R., Fulcheri, L. (2007). A comparative study of non-thermal plasma assisted reforming technologies. *International Journal of Hydrogen Energy 32(14)*, 2848-2867. https://doi.org/10.1016/j.ijhydene.2007.03.026

Sanders, J., Clark, J., Harmsen, G., Heeres, H., Heijnen, J., Kersten, S., van Swaaij, W., Moulijn, J. (2012). Process intensification in the future production of base chemicals from biomass. *Chemical Engineering and Processing: Process Intensification 51*, 117-136. https://doi.org/10.1016/j.cep.2011.08.007

Santos, C. A., Phuong, N. H., Park, M. J., Kim, S. B., Jo, Y. M. (2020). Decomposition of indoor VOC pollutants using non-thermal plasma with gas recycling. *Korean Journal of Chemical Engineering 37(1)*, 120-129. https://doi.org/10.1007/s11814-019-0406-8

Soto, G., Pahuamba, E., Ramírez, F., Cruz-Reyes, J., del Valle, M., Tiznado, H. (2019). Swirling fluidized bed plasma reactor for the preparation of supported nanoparticles. *Revista Mexicana de Ingeniería Química 19(2)*, 867-875. https://doi.org/10.24275/rmiq/Mat886

Soto-Ruvalcaba, L. (2014). *Development of a System for Plasma Generation Base on a Coplanar Dielectric Barrier Discharge*. Master thesis in Advanced Technology, Instituto Politécnico Nacional, Mexico, http://tesis.ipn.mx/handle/123456789/13135

Sperandio, L., Colombo, M., Andrade, C., Costa, C. (2022). The Development of a low-cost portable turbidimeter for chemical processes. *Revista Mexicana de Ingeniería Química 21(1)*, Proc2559. https://doi.org/10.24275/rmiq/Proc2559

Stankiewicz, A. I., Moulijn, J. A. (2000). Process intensification: transforming chemical engineering. *Chemical Engineering Progress 96(1)*, 22-34.

Taghvaei, H., Shirazi, M. M., Hooshmand, N., Rahimpour, M. R., Jahanmiri, A. (2012). Experimental investigation of hydrogen production through heavy naphtha cracking in pulsed DBD reactor. *Applied Energy 98*, 3-10. https://doi.org/10.1016/j.apenergy.2012.02.005

Tian, Y., Demirel, S. E., Hasan, M. F., Pistikopoulos, E. N. (2018). An overview of process systems engineering approaches for process intensification: State of the art. *Chemical Engineering and Processing - Process Intensification 133*, 160-210. https://doi.org/10.1016/j.cep.2018.07.014

U.S. Energy Information Administration. (2021). *Short-Term Energy Outlook - U.S. Energy Information Administration (EIA)*. Energy Information Administration. https://www.eia.gov/outlooks/steo/report/global_oil.php

Vandenbroucke, A. M., Morent, R., de Geyter, N., Leys, C. (2011). Non-thermal plasmas for non-catalytic and catalytic VOC abatement. *Journal of Hazardous Materials 195*, 30-54. https://doi.org/10.1016/j.jhazmat.2011.08.060

Wang, H., Mustaffar, A., Phan, A. N., Zivkovic, V., Reay, D., Law, R., Boodhoo, K. (2017). A review of process intensification applied to solids handling. *Chemical Engineering and Processing: Process Intensification 118*, 78-107. https://doi.org/10.1016/j.cep.2017.04.007

Wang, L., Liu, S. Y., Xu, C., Tu, X. (2016). Direct conversion of methanol to n-C_4H_{10} and H_2 in a dielectric barrier discharge reactor. *Green Chemistry 18(20)*, 5658-5666. https://doi.org/10.1039/c6gc01604a

Yaws, C. (2015). *The Yaws Handbook of Vapor Pressure: Antoine Coefficients*. (2nd Revised ed.). Gulf Professional Publishing.